LAL/RT 90-09
June 1990

Laboratoire de l'Accélérateur Linéaire

CONTRIBUTIONS TO THE 2nd EPAC CONFERENCE

E P A C
European Particle Accelerator Conference
Nice, 12–16 June 1990

U.E.R
de
l'Université Paris-Sud

Institut National
de Physique Nucléaire
et
de Physique des Particules

Bâtiment 200 - 91405 ORSAY Cedex

LAL/RT 90-09
June 1990

CONTRIBUTIONS TO THE 2nd EPAC CONFERENCE

Operational limits of high accelerator gradients
G. Bienvenu, P. Brunet

Electron gun for the FEL CLIO
R. Chaput

A high accuracy programmable timing system for the Linac
of the CLIO free electron laser
E. Plouviez, C. Eder

LAL (Orsay) RF gun project
C. Travier, J. Gao

Presented at the European Particle Accelerator Conference
Nice, 12–16 June 1990

OPERATIONAL LIMITS OF HIGH ACCELERATOR GRADIENTS

G. BIENVENU P.BRUNET

UNIVERSITE PARIS-SUD -Laboratoire de l'Accélérateur Linéaire-
Bâtiment 200 , 91405 ORSAY, Cedex - FRANCE-

Abstract. We report in this paper the experimental results of two S band warm accelerating structures under high gradient. Routinely a field higher than 40 MVm^{-1} has been obtained with long RF pulses and 80 MVm^{-1} for short pulses. We give also the shape and the spectral analysis of dark electric charges, the level of self-emitted charges, per unit length are plotted as function of surface field.

INTRODUCTION

High accelerating field are needed for future accelerators. For an accelerating electric field typically of 100 $MeVm^{-1}$ many problems occur, such as breakdown and dark current. For this reasons the Laboratoire de l'Accélérateur Linéaire carry on a R & D programme on high accelerating structures. 4 years ago LAL has built a high gradient test facility *NEPAL* composed of a high RF power source,a relativistic electron source and an analysis zone,The experimental structure is laid between them.

This paper report a part of the experimental results, under a very pratical point of view, carried on two S band disk loaded warm structures.

STRUCTURES UNDER TEST

Two types of accelerating structures are presently under test :

- A short section derived from the end landing of *LIL*[1] structure, specially designed for high axial electric field.
- A new type of S band structure[2] developed by *GE/CGR – MeV* company with the collaboration of *LAL*

The main characteristics of these structures are summarized in the table I.

STRUCTURES PARAMETERS		
Structure	SERA	CGR
Frequency, f (Mhz)	2998.5	2998.5
Operating mode	$2\pi/3$ Dir	$4\pi/5$ Back
Structure type	TW, C^{te} imp.	TW, C^{te} imp.
Cell shape	iris	nose cone
Coupling	electric	magnetic
Tuning	wall deformation	stub
Length, L (m)	0.504	1.270
Factor of merite, Q	14600	11100
Shunt impedance, r (MΩ/m)	64.24	75.0
Filling time, τ (μs)	0.297	0.203
Relative fondamental harmonic, T	0.90	0.85
Attenuation, X (Np)	0.196	0.172
Groupe velocity, v_g (m/s)	$6.4^{-2}c$	$21.2^{-2}c$
Peak axial field, $\hat{E}_{oa}$ (MV/m)	$6.8\sqrt{P}$	$5.04\sqrt{P}$
Average axial field, $\overline{E}_{oa}$ (MV/m)	$6.2\sqrt{P}$	$4.66\sqrt{P}$
Average accelerator field, $\overline{E}_{oca}$ (MV/m)	$5.57\sqrt{P}$	$3.95\sqrt{P}$
Ratio max surface field/axial field	1.9	2.6

Table I

BREAKDOWN IN STRUCTURES.

Two levels of breakdown has been fixed arbitrary

- An operational level, corresponding to a number of breakdown

$$\leq 3 \quad 10^{-4} s^{-1}$$

(roughly one breakdown per hour)

- A limit level corresponding to

$$\leq 3 \quad 10^{-2} s^{-1}$$

(roughly one breakdown per 30 s)

Behavior with the length of rectangular RF pulse

We assume that time dependence of the peak surface field (averaged over the structure length), is :

$$\overline{E}_s = \frac{K}{\tau^{\alpha}}$$

The experimental values of K and α are given in table II , for $\overline{E}_s$ in MVm^{-1} and τ in μs were τ is the pulse length.

We can noticed that the value of α is the same for the two sections .

Structure	LIL	CGR
α	0.2	0.2
$K_{lim.}$	100	88
$K_{op.}$	95	84

Table II

Maximal electric field with compressed RF pulses

For $SLED^3$ RF pulses, operational and limit values of electric surface field are given in the table III.

The timing of the compressed RF pulse is ajusted for eliminating the multipactor phenomenon yielded by the low power inverse queue. The values given by the table are probably partly limited by the poor vacuum level in the RF window region ($5\ \ 10^{-7} mbar$).

Experimentally obtained gradients With M.P.G.				
	Limit 3.10^{-2}/s		Operational 3.10^{-4}/s	
Structure	LIL	CGR	LIL	CGR
$\hat{P}$ (MW)	168	168	139	125
$\overline{E}_{os}$ (MV/m)*	80	55	73	42
$\hat{E}_{os}$ (MV/m)	88	68	80	58
E_s (MV/m)	153	109	130	120
$\hat{E}_s$ (MV/m)	167	177	152	153

* calculated with input power

Table III

DARK CURRENT

Dark current with rectangular RF pulse

The dark current shape as function of time is given by the photography 1. On the figure 2, the spectral analysis of this current is plotted. The first peak corresponding to the lower energy ($\leq 3\ \ MeV$) is connected with the forehead of RF wave, its length is equal to the filling time of the section. The second pic and the last one are due to an overfield bound with reflected waves, and the flat region is the steady state regime.

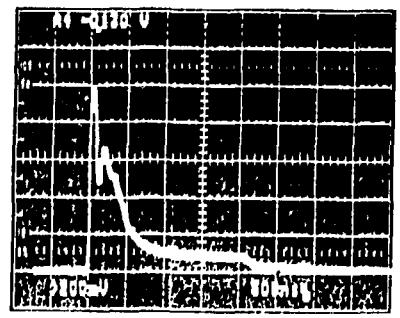

Fig 1

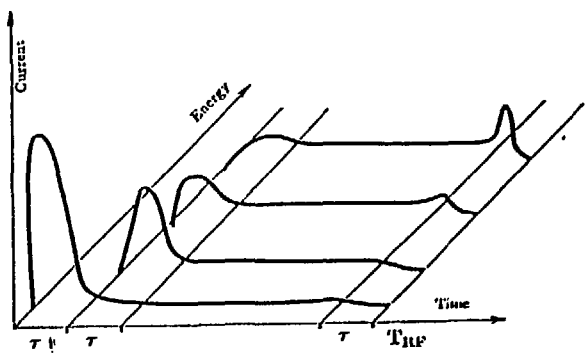

Fig 2

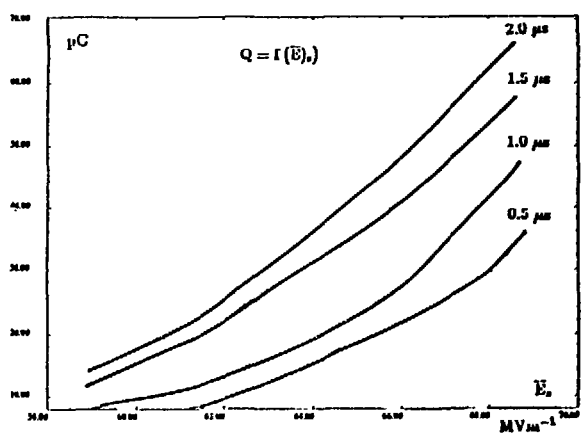

Fig 3

Electric charges

Dark electric charges are reported for different rectangular RF pulses length on the figure 3 for the section *LIL*.

The electric charge is roughly proportional to :

$$Q_{dc} = \overline{E}_a^{5.5}$$

Dark current with compressed RF pulse

The shape of dark current in compressed mode is given, for the section *CGR* on the figure 4. The photo has been recorded from a well adapted coaxial faraday cup. The dark electric charge per length unit is plotted, on the figure 5, as function of average surface field. We see that the nose cone *CGR* structure yields more dark current that the usual disk structures.

Spectrum of dark current

The spectrum of the dark current extendes from zero to the maximum of energy gain, with an maximal amplitude on the middle range of energy. The spectrum of figure 6 corresponds to the *LIL* structure, and an identical shape will be reported with the *CGR* section.

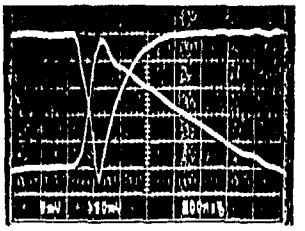

Fig 4

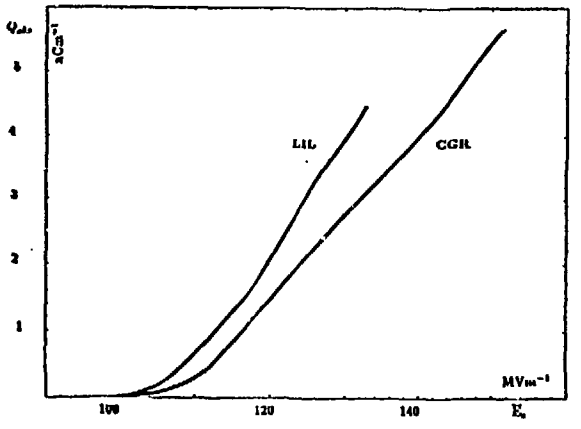

Fig 5

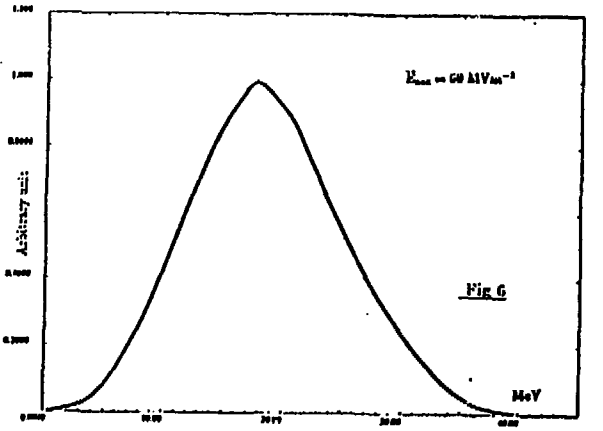

Fig 6

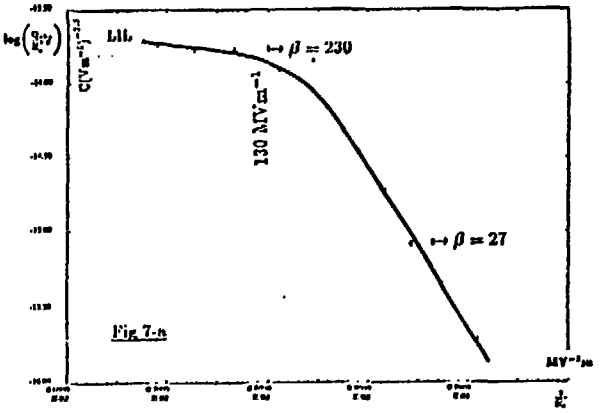

Fig 7-a

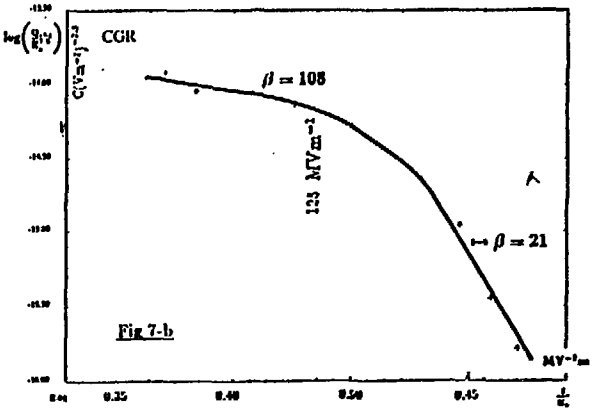

Fig 7-b

FOWLER NORDHEIN PLOTS

Figures 7-a and 7-b report F.N plots of the two sections. These curves are plotted with the dark electric charge and the average of the peak surface field. We notice around 230 MVm^{-1} a quite sharp change in F.N curves slopes in connection with a decreasing of field electronic emission.

REFERENCES

(1) R Belbeoch et al. Rapport d' étude sur le projet des linacs injecteurs de *LEP* LAL/RT/82-01 jan 82

(2) D Tronc , IEE Trans.Nucl.Sci., NS 32 (1985) 3243

ELECTRON GUN FOR THE FEL CLIO

R. Chaput
Universite Paris-Sud, Laboratoire pour l'Utilisation du Rayonnement Electromagnétique
Bâtiment 209 D - Centre Universitaire Paris-Sud
91405 Orsay, Cédex, FRANCE

Summary

A triode electron gun has been developped and manufactured at LURE (Laboratoire pour l'Utilisation du Rayonnement Electromagnétique) and LAL (Laboratoire de l'Accélérateur Linéaire) for the free electron laser CLIO[1] (Collaboration pour un laser à électrons libres dans l'infrarouge à Orsay) now under construction : this gun involves a grid-cathode assembly manufactured by EIMAC, currently used in the SLAC gun family.

For the FEL requirements, the gun must be able to yield a train of shorts pulses at accuracy frequency or a continuous pulse.

Driving together the cathode and the grid the gun produces a continious beam of 12 µs or a pulsed beam of very short pulse of 1 ns at 250 MHz, 125 MHz, 62.5 MHz or 31.25 MHz. The performances of the gun has been tested on a testing bench. A peak current of 1 Amp. for 1 ns width at any frequencies was achieved at an injection voltage of 90 kV.

Introduction.

The free electron laser CLIO is designed to be broadly tunable in the infrared range from 2 to 20 µm with an average power of 10 to 100 W.

It is driven by a S band Linac of 50 to 80 MeV that yields some micropulses of 1 nC (100 Amp., 10 ps) at the frequency required for the laser (even multiple of 31.25 MHz up to 500 MHz). By the subharmonic bunching process the gun must produce only 1 Amp., 1 ns pulses every 4, 8, 16 or 32 ns during all the 12 µs macropulse in synchronism with the R.F. frequency at 500 MHz of the subharmonic cavity.

A peak gun current of 1 Amp. to 1.5 Amp. was aimed with a width shorter than a half period of the RF frequency i.e FWHM
< 1ns in order to avoid too larges parasitics bunches.

Electron gun

This gun is called "SLL gun" from SLAC for the original design[2], LAL and LURE for the development and manufacture. This gun is a classical Pierce gridded gun with a thermoelectronic dispenser cathode. Mechanically the gun frame is designed to fit several cathodes manufactured by EIMAC. The Y 646 B, Y 845 or Y 796. This later model will be used in a further version of our FEL. The gun structure is shown in Fig. 1. At this time we use the Y 646 B model, the cathode has a 8 mm diameter and the grid-cathode spacing is 0.15 mm with a screening fraction of about 15% to 20%.

Keeping the filament voltage and current at their nominales values 6.3 V and 1.4 Amp., the peak cathode current can reach up to 2.5 Amp. for a grid-cathode net drive of 70 V.

Like we need only 1 Amp. to 1.5 Amp. this cathode is sufficient. The gun electrode geometry was modeled using the "ETP Hermannsfeldt code" of SLAC[3] in order to get the smallest emittance for 90 kV and 1.5 Amp. The code predict an emittance $\varepsilon^N = 2\ \pi$ mm mrad very close to the cathode emittance alone. However for smallest currents the emittance grows.

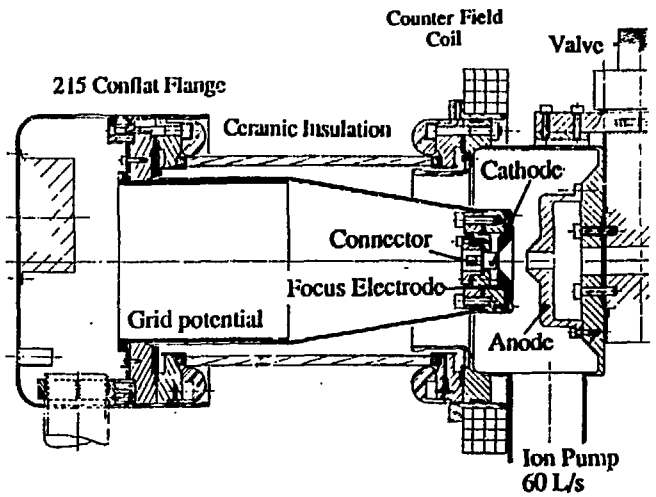

Fig. 1 Structure of the gun assembly

We have roughly evaluated the grid lens effect and finally estimated a normalized emittance $\varepsilon^N \approx 15\ \pi$ mm mrad in the range of 0.5 Amp. to 1.5 Amp. at 90 kV.

The distance between the cathode and anode is 24 mm and the anode hole diameter is 8 mm. At the cross over the beam diameter is 2.6 mm. Fig. 2 shows the calculated beam trajectories.

The ceramic isolator is designed to withstand up to 200 kVDC. Each side is brazed on a 215 conflat flange surrounded by anticorona rings. This ceramic isolator was especially manufactured by SCT CERAVER France.

The vacuum chamber is large enough to receive another set of more large electrodes used with the 4796 cathode.

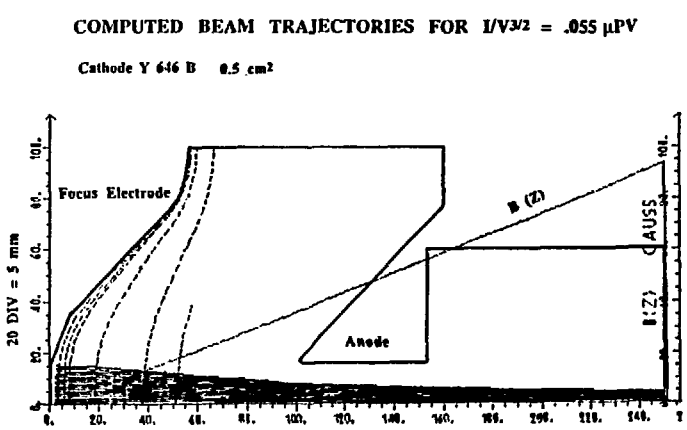

Fig. 2 Computed beam trajectories from the cathode to the cross over

The cathode anode space is pumped down through a good conductance pipe of diameter 65 mm by a 60 l/s ion pump. The pressure while the gun is running is between 10^{-8} and 10^{-9} Torr. This pressure is sufficiently low for a dispenser cathode. Directly on the gun chamber a gauge monitor the pressure.

All the pieces under vacuum that must withstand a high electric field have been polished and baked before assembly. And a last baking of the whole gun was performed at 180°C to reduce the water vapor more than 36 hours. The process of cathode activation was started when the pressure fell under 10^{-6} Torr. The high voltage conditioning was performed up to 100 kVDC for a nominal rating value of 90 kV, with a serial resistor of several meghoms in order to avoid too severe sparks between electrodes.

A counter-field coil located in the cathode plane cancel the residual magnetic field from the air coil on the Linac. Inside the gun the magnetic field increases from zero at the cathode with a gradient of 1 k Gauss/meter.

Pulser system.

The triode gun is driven by the cathode and the grid. In the "CW mode" the grid alone drives the triode with a large positive pulse of 12 µs 100 V. The pulse width is controled from the ground level by optical link.

In the pulsed mode, a 500 MHz 2 W signal during 16 µs is carried to the high voltage deck throught an isolated HF transformer made of two coupled loops of H.V. isolated cable, with an insertion loss of -3dB. A frequency divider (very fast ECL technology from PLESSEY) controled from the ground level throught optical links, elaborates the pulsed signal of 0.9 ns width every 4, 8, 16 or 32 ns which will be amplified in negatives pulses up to -110 V/1.2 ns by a wideband solid state amplifier 10 - 500 MHz, and applied on the cathode. This power amplifier has been especially developed for yield negative pulses as short as possible, by NUCLETUDES S.A. a French manufacturer.

In the same time the grid pulse of adjustable duration is used for doing a window that eliminate the first microsecondes while the power amplifier has small amplitude oscillations.

With a minimum grid bias of -20 V, beam micropulses of 1.5 Amp./1.4 ns were achievied.

Along the 12 µs, the residual macropulse amplitude droop is compensated by an adjustable counter voltage slope applied on the grid up to ± 10 mA/µs.

The average cathode and grid currents are monitored by two currents transformer on their connexions, and measured from the ground level by the way of analogical opto-link.

In the "CW mode" the total charge aimed in the macropulse is 6 µC (0.5 Amp. 12 µs) a 15 nF buffer capacitor in the H.V. supply yields this charge and keep constant the high voltage at 4 x 10^{-3}. Fig. 3 shows a block diagram of the modulator.

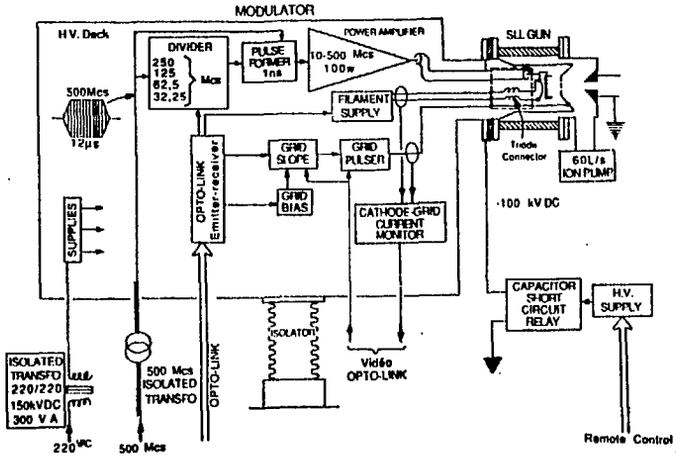

Fig. 3 Block diagram of the high voltage deck modulator

Control

The gun modulator is remote controlled by a 68008 MOTOROLA microcomputer in G 64 standard crates. From the control room, a program automatically starts the gun and put the parameters at their rating values.These program are wrote in C language.

Characteristics of the electron gun.

The cathode and grid currents are measured on long pulse 12 µs from the H.V. deck modulator by an analogical opto-link.

On the testing bench the beam current has been measured by a coaxial target and a cylindrical pick up electrode. The target has a characteristic transfert impedance of 10 Ω and allow to measured both short or long pulses, but the current absolute value may be disturbed by a secondary emission. For a more accurate measure we use the cylindrical pick up electrode which no intercepte the beam, its sensitivity is 0.5 V/Amp. for a beam of 90 keV.

A 7104 Tektronix oscilloscope 1 GHz bandwidth was used because the low repetition rate of 1 to 50 Hz.

The figure 4 shows the cathode emission characteristics as a fonction of filament voltage in the range of 1.5 Amp. of cathode current with a grid net drive of 30 V. At 6.3 V filament voltage, the gun works in space charge region and at this cathode temperature the dark current emitted by the grid is lower than 0.1 µAmp., but it rapidly increases for filament voltage upper to 7 V.

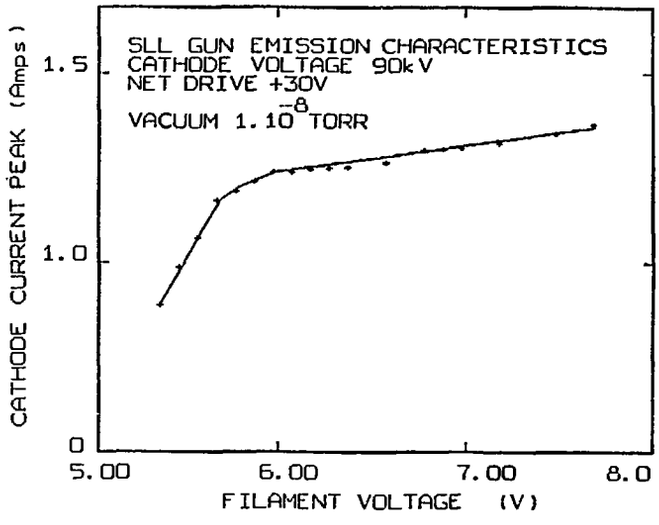

Fig. 4 Emission characteristics of the dispenser cathode Y 646 B

In the space charge rate, the cathode current follows the general equation of triode $I_K = G(Vg + Vp/\mu)^{3/2}$ with an amplification factor $\mu \approx 10^4$ and a perveance $G \approx 5.2 \times 10^{-3}$ A/V$^{3/2}$. The cut off amplification factor is µ C.O. ≈ 6600.

The grid interception or screening fraction depends of the grid and anode/cathode voltages for 90 kV anode potential, it increases about lineary with the cathode current from 12% at 0.5 Amp. up to 21% at 2.6 Amp.

The Fig. 5 shows the transfer characteristics in short pulses at filament voltage 6.3 V the maximum anode current available is limited by a perveance of 0.15 µAmp./V$^{3/2}$.

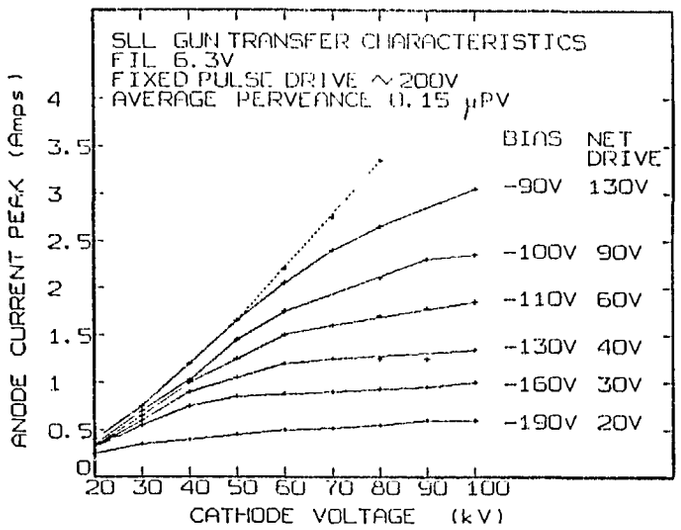

Fig. 5 Gun transfer characteristics in short pulse of about 1 ns

Fig. 6 shows the wave form of a short pulse beam during the 12 μs macropulse. It has been measured by the pick up electrode and the 7104 oscilloscope with a time resolution measured of 370 ps. For 1 Amp. peak the rise time is 470 ps and 1.1ns (FWHM).

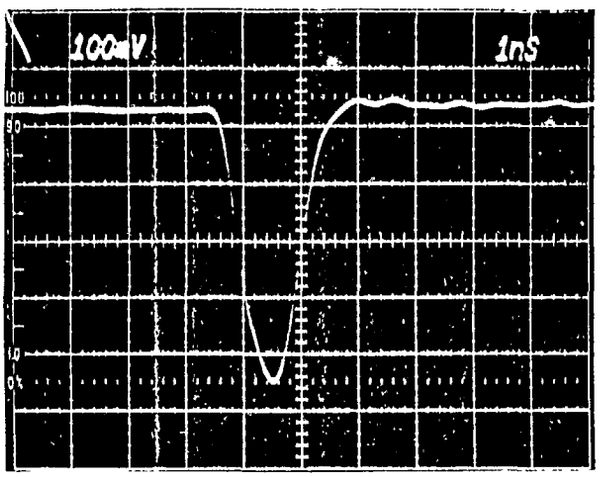

Fig. 6 Pick up electrode signal, waveform of a short pulse of 1 Amp. peak 470 ps rise time and 1.1 ns (FWHM)

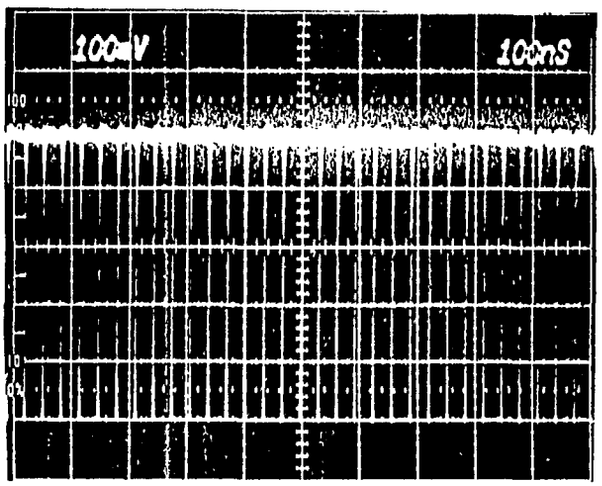

Fig. 7 A part of the micropulses train at 31.25 MHz, 1 Amp. peak, 12 μs duration.
Flat top stability < 0.5%

Fig. 7 shows a part of the micropulses train at 31.25 MHz. The flat top ondulation is lower than 0.5% on the 12 μs total duration.

The phase shift between the gun micropulses and the original 500 MHz from the RF subharmonic cavity is lower than 1°.

Aknowledgements

I am grateful to all the people of the CLIO team for their wide contribution in this project.

References

[1] Rapport CLIO LAL/RT 89-04 - February 1989.

[2] One nanoseconde pulsed electron gun systems
Roland F. KOONTZ SLAC - PUB - 2261
February 1979.

[3] W.B. Herrmansfeldt, "Electron Trajectory Program" SLAC report 226, November 1979.

A HIGH ACCURACY PROGRAMMABLE TIMING SYSTEM FOR THE LINAC OF THE CLIO FREE ELECTRON LASER.

Eric Plouviez, Claude Eder,
Laboratoire de l'Accélérateur Linéaire, IN2P3-CNRS et Université de Paris-Sud,
F-91405 Orsay, Cedex, FRANCE

In order to allow a very good repeatability of the operation of the linac of CLIO, a low jitter triggering electronic has been built. This electronic is based on the use of programmable preset counters synchronised by a clock derived from the pilot of the RF. The circuits are implemented on Europe boards and programmed with a G 64 bus. A basic circuit synchronised with a 31.25 MHz clock allows the programmation of triggering signals in a 2 ms range by steps of 32 ns with less than 50 ps jitter. For more stringent applications an additional circuit synchronized on a 500 MHz clock is used. This circuit is built using a 500 MHz varicap phase shifter, a HP HDMP 2001 retiming circuit and an Analog Device AD 9500 programmable delay generator. It allows the generation of 500 ps risetime pulses with less than 10 ps jitter and 10 ps repeatability with respect with the linac's beam, inside the same 2 ms range.

Introduction.

CLIO is a free electron laser driven by a 60 MeV linac.The linacs RF frequency is 2998.55 MHz ; the electron bunches will be produced in an injector composed of a thermionic gun followed by two bunching RF structures with 499.76 and 2998.55 MHz RF frequencies. The linac will be operated in 12 µs long RF pulses with a repetition rate of 50, 25, 12.5, 6.25 Hz. Inside this 12 µs pulse length the spacing between the electron bunches will be n x 2 ηs (n = 1 to 16) and the bunches length about 15 ps : the thermionic gun will provide 1 ηs bunches and the subharmonic buncher will compress this length to less than 180° of phase of the 2998.55 MHz bunchers RF frequency ; this length will be reduced down to 15 ps in the S band buncher. The operation of the laser will demand a very good stability of the operating parameters of the RF. In order to contribute to this stability the timing system of the pulsed element of the machine and their associated measurement electronics has been designed in order to avoid any variation of the operating parameters due to jitter or long time drift. The timing system has also been designed in order to be flexibly controlled by the G 64 bus used for the control CLIO.

32 ηs steps G 64 programmable pulse generators.

Most of the timing requirements of CLIO components can be met with a resolution of about 50 ns for the delay and width of the pulses. These requirements are due the risetime of the pulsed RF generators, filling time of the RF structures, bandwidth of the electronics etc. The most used approach to build a programmable timing pulse generator with low jitter and good accuracy is to use programmable synchronous preset counters circuits with high stability clock and reset signals. We wanted to implement this circuits on a G 64 format board using G 64 standard power supplies.The fastest preset counters IC compatible with this approach are the 74 AS serie 74 ALS 867 8 bits counters with a maximum clock frequency of 50 MHz. The subharmonic frequency of the 499.76 MHz immediatly inferior is 31.235 MHz (32 ηs period). With a 16 bits programmation of the delay and width of the pulses and this clock frequency we cover a 2.097 ms range in 32 ηs steps for both settings which is more than enough for our applications.
In addition to the programmation of the delay and length of the pulses it is also possible to choose the rate of the generation of the pulse (50, 25, 12.5, 6.25 Hz) and single shot and to use an internal 31.235 MHz clock for stand alone operation of the module. One connector of the bus can be used to program one or two pulse generators. These G 64 modules will be implemented in the different G 64 crates controlling the CLIO components and will be synchronized by the same reset and clock signals.

Generation and distribution of the reset and clock signal

The 31.235 MHz clock signal is generated with ECL D flip flops dividing the frequency of the 499.76 MHz subharmonic bunchers RF pilot frequency. The 499.76 MHz pilot is a state of the art transistor cavity oscillator phase locked on an oven temperature stabilized quartz reference at 99.951 MHz. The stability of the reference is better than 5.10^{-9} per day. Both the phase locked source and the quartz reference are commercially available components.The repetition rate of the operation of CLIO is the 50 Hz AC frequency and its subharmonics. The timing reset pulse is generated a quarter of period after the positive zero crossing of the AC main voltage. The amplitude of the next positive half period of the 31.235 MHz following this reset signal is doubled according to the following time diagram.

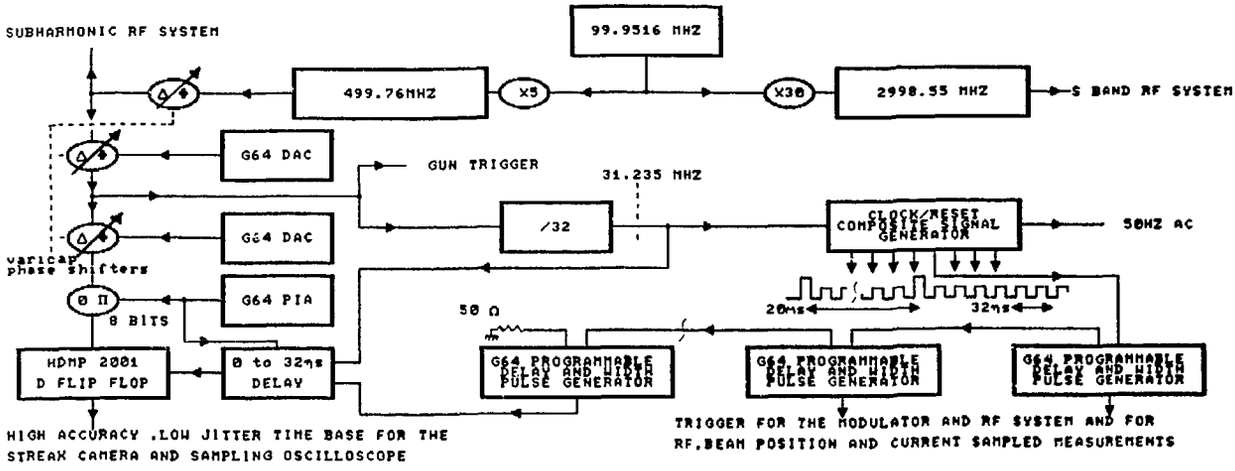

Figure 1 : Schematic diagram of the timing system of CLIO

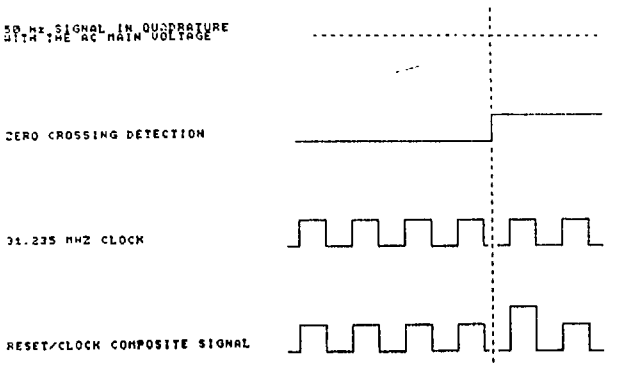

Figure 2 : timing diagram of the clock/reset composite signal generation

This signal is amplified and multiplexed in order to be available at eight outputs with an amplitude of 1 volt on 50 Ω (2 volts for the reset pulse). In this way the preset and the clock signals for the G 64 modules are available on the same cable. Up to five G 64 modules can be daisy chained along a cable delivering the signal on a distance much longer than the CLIO dimensions.

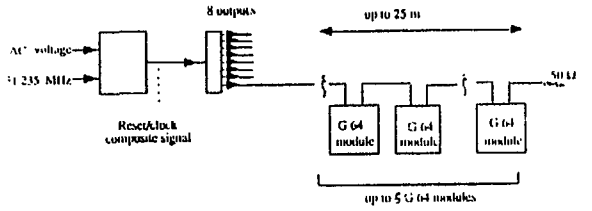

Figure 3: Interconnection of the 32 ns steps timing system components

High accuracy timing circuit.

For some application we need a time base with a more precise setting and a lower jitter. We will use a streak camera, a fast digitizer and a sampling oscilloscope for measurements of the bunched beams micropulses parameters (length, parasite satellites bunches, etc). A convenient and flexible approach to trigger these instruments would be to use a time base synchronized on the RF signal and programmable with a good resetability. The most stringent application is the triggering of the streak camera which demands a jitter inferior to 10 ps (our streak camera trigger input signal must be a 4 volts 1 ηs rise time, 30 ηs long signal).

Principle of the circuit.

This high resolution programmable delay signal is generated with a D flip flop circuit using the 499.76 MHz signal as a clock. To set precisely the delay of the output pulse we change the phase of the clock signal using electronic phase shifters and we select the right period of the clock using the D input for the long range delay setting according to the figure 4. The varicap phase shifter does not introduce any additional jitter (providing the control voltage is not noisy) and is easy to control with a DAC. Using the classical circuit given below we get a 0 to 200° range of phase shift. An additional phase inverter made of another 3 dB hybrid terminated by an ASGA switch increases the phase shift range of 180° (figure 5 photograph) giving a 2 ηs range for the fine setting of the delay.

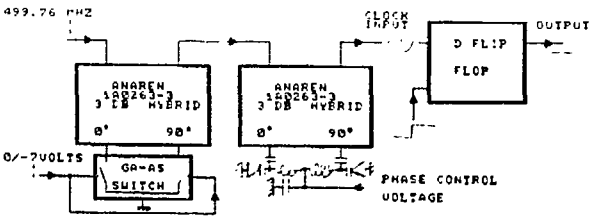

Figure 4 : D flip flop and phase shifters arrangement

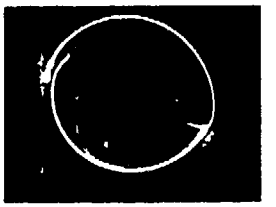

Figure 5 : Phase shifters range measurement (amplitude/phase polar display)

Choice and evaluation of the D flip flop.

In order to have a reliable operation at 499.76 MHz and a low rise time of the output we have decided to use a circuit able to operate with a clock frequency of 1.5 GHz. Our two main concerns were the stability of the propagation delay between the clock input and the output and the insensitivity of this delay to the position (and jitter)of the D input signal leading edge. The circuit that we have tested is an HDMP 2001 developed for the synchronisation of high rate digital communication data links.

Clock input to output delay measurement.

The delay jitter was measured using a jitter free 31.235 MHz signal, subharmonic of the 499.76 MHz clock as the D input signal. The 31.235 MHz signal generated at the output was used as an external trigger for a sampling oscilloscope and the 2998.55 MHz 6th harmonic of the clock signal (for better sensitivity) visualised on the oscilloscope as shown on figure 6.

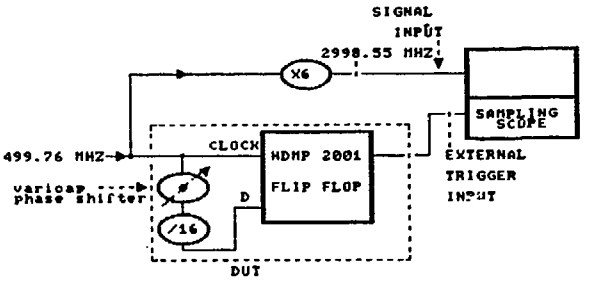

Figure 6 : Delay and jitter measurement

With the right D input phase shifter setting no measurable jitter was observed. The drift of the output signal for temperature variation, measured on the same set up was found to be less than 10ps for a 50° variation of temperature.

We have also measured the variation of the clock input to output delay with respect to the D input signal position (by varying the setting of the phase shifter). The result of the measurements are given on the curve below.

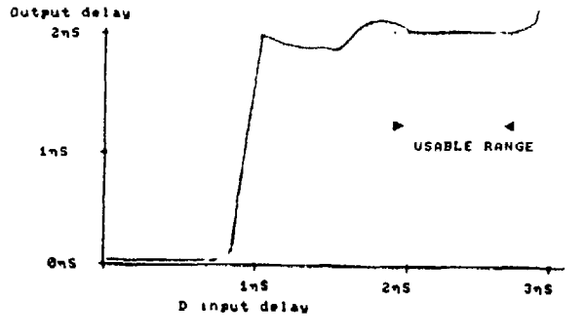

Figure 7 : HDMP 2001 clock rising edge to output delay versus D input to clock rising edge delay

The important point for our application is that there is a 700 ps range where the output pulse is insensitive to small jitters at the D input.

Generation of th D input signal.

To fill the gap between this 2 ηs range and the 32 ηs steps width of the G 64 pulse generator described above we use an AD 9500 integrated circuit made by Analog Device [2] This circuit allow the programmation with 8 bits accuracy of its output pulse with respect to a trigger pulse. The range of the delay programmation is given by the choice of the values of a set of external resistor and capacitor for our application this range is of course 32 ηs . The jitter of the output pulse for this delay range is about 100 ps. The input and output levels are ECL and the output rise time is 2 ηs For our application the circuit is triggered by one of our G 64 pulse generator and the output signal is used to validate the D input of the D flip flop clocked by the 499.76 MHz.

Operation of our circuit.

The complete schematic diagram of our circuit is given below.

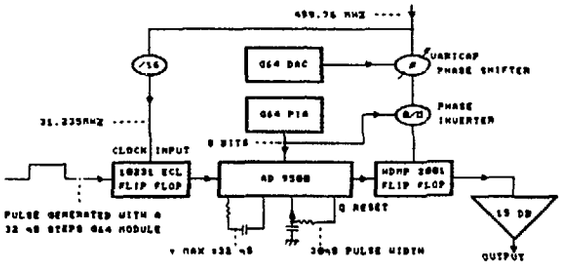

Figure : 8 Schematic diagram of the high accuracy time base circuit

The 31.235 MHz subharmonic of the 499.76 MHz is used to resynchronize the leading edge of the pulse generated by the G 64 module. This frequency is used instead of the 499.76 MHz because of the relatively high 20 ηs rise time of the output of the G 64 module. The output signal of the 10131 ECL flip flop has a 5 ηs rise time with a constant position with respect to the 499.76 MHz clock of the HDMP 2001 This signal triggers the AD 9500 The five most significant bits of the AD 9500 programmation inputs are set in order to select the proper 2 ηs period inside the 32 ηs step of the G 64 pulse generator. The fine setting of the delay is then obtained by the programmation of the varicap phase shifter and 0/π phase inverter. In order to generate an output pulse with the lowest jitter we program the three least significant bits of the AD 9500 programmation inputs to have the proper delay between the signals leading edges at the clock and D inputs of the HDMP 2001.
The value of the programmation bits of the G 64 module, of the AD 9500 circuit and of the DAC driving the varicap phase shifter for a given delay are calculated by a program writen in C and running on the local controller of the G 64 bus.

Test results.

The delay of the signal generated by our circuit can be continuously varied in a 2 ηs range with respect to a time reference. The accuracy of the setting is function of the circuit and of the reference signal : we have measured the contribution of our circuit to the jitter of the CLIO time base using again the set up of the figure 6. Figures 9a and 9b show the 6th harmonic of the 499.76 clock measured on a Tektronix 11800 sampling scope externaly triggered on figure 9a by a jitter free signal and on figure 9b by the output of our time base : the additional jitter due to our circuit on figure 9b is less than 10ps

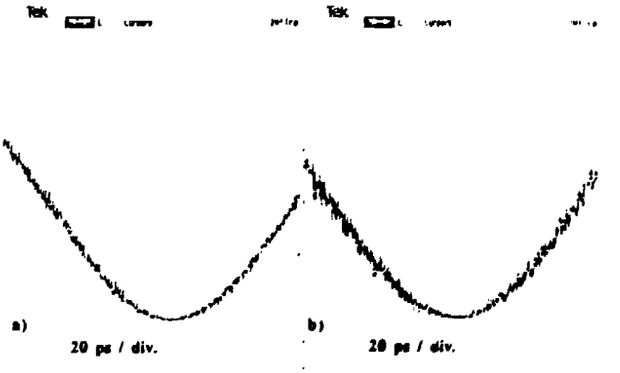

Figure 9 : 6th harmonic of the 499.76 MHz clock visualised with a sampling scope triggered by a jitter free signal (a) and by our high accuracy timing circuit (b).

Aknowledgements :

The authors thank M. BERNARD for his contribution to the writing of the control code for G 64 modules and to the improvement of the fast electronic circuit and J.C. JUMEL for his help in the development of the clock generator.

References :

[1] First beam of the CLIO linac, J.C. BOURDON, LAL, this conference.

[2] Hewlett Packard : Decision circuit, HDMP 2001, technical data, september 1988.

[3] Analog Devices : AD 9500, digitally programmable generator. Analog products data book, 1989.

LAL (ORSAY) RF GUN PROJECT

C. Travier
Laboratoire de l'Accélérateur Linéaire
Bât. 200, Centre d'Orsay
91405 ORSAY Cedex, FRANCE

J. Gao
visitor from IHEP
P.O. Box 2732, Beijing 100080, CHINA

Abstract

A two-cavity RF gun basic design is presented. The electric field distribution along the beam axis is chosen to minimize emittance growth. Independent phasing of the cavities allows to minimize energy spread. Simulations with the codes PARMELA [1] and PRIAM [2] are presented. According to this design, a low-level model cavity was launched.

Introduction

As part of the LAL/Orsay R & D program on future e^+e^- linear colliders [3], an RF gun design was started at the beginning of 1990.

Originally proposed by G.A. Westenkow and J.M.J. Madey [4], the RF gun concept is now widely studied and experienced. Both thermionic [4-6] and laser-driven [7-15] RF guns are now under construction, test or operation around the world.

The cathode being located in a high-gradient RF cavity, the electrons experience a high accelerating field and are thus less sensitive to space charge forces. In case of laser-driven RF guns, very short pulses can be produced by illuminating high-current density photocathodes with picosecond lasers. These properties result in high-brightness electron sources well suited for e^+e^- linear colliders, FEL injectors and synchrotron radiation storage ring linear injectors.

At Orsay, the goal of this development on RF gun is to gain some experience in this field while providing a possible high-brightness gun for the accelerator test-facility NEPAL [16]. The chosen operating frequency is thus 3 GHz. A dispenser cathode will be used, therefore allowing both thermionic and laser-driven operation [17].

Theoretical investigations showed that two-cavities independently powered and phased would allow to minimize both emittance and energy spread. Longitudinal electric field profile with RF focusing was chosen for the first cavity.

Beam dynamic simulations were conducted using both PARMELA and PRIAM codes. Many parameters can be varied: accelerating field in both cavities, RF phase for laser pulse, phasing of the cavities, pulse length, current, laser spot size, laser profile. Results presented here are partial and do not cover all the possible range of investigations.

Theoretical investigation

In an RF gun, electron beam is subject to several effects that contribute to energy spread and emittance growth [18]: space charge forces both linear and nonlinear, nonlinear time-independent field effects and linear time-dependent RF field effects which are characteristic of RF guns when compared to DC guns. To minimize emittance growth, there are at least two criteria: one is to minimize nonlinear field effects [19,9] (by designing a cavity with linear radial fields and by taking a beam diameter small enough), the other is to minimize linear time-dependent RF field effects [20].

Assuming that a cavity has a cylindrical symmetry, the electric field $E_z(r,z,\varphi,t)$ can be written $E_z(r,z)\sin(\omega t+\phi_0)$. Maxwell equations allow then to express the electromagnetic fields off axis ($E_z(r,z)$, $E_r(r,z)$, $H_\varphi(r,z)$) as a function of the longitudinal on axis electric field $E_z(0,z)$. The transverse force F_{rrf} applied to a particle of charge q and velocity v_z is expressed by $F_{rrf} = qE_r - q\mu_0 v_z H_\varphi$. It can then be written as:

$$F_{rrf} = -\frac{qr}{2}\left(\frac{dE_z(0,z)}{dz}\sin(\omega t+\phi_0)+\epsilon_0\omega v_z E_z(0,z)\cos(\omega t+\phi_0)\right)$$
$$+\frac{qr^3}{16}\left(\left(\frac{d^3E_z(0,z)}{dz^3}+k^2\frac{dE_z(0,z)}{dz}\right)\sin(\omega t+\phi_0)+\right.$$
$$\left.\mu_0\epsilon_0\omega v_z\left(\frac{d^2E_z(0,z)}{dz^2}+k^2E_z(0,z)\right)\cos(\omega t+\phi_0)\right)+h(r^5)+\cdots \quad (1)$$

where $\omega = kc$. If space charge forces F_{rsc} are considered, then

$$F_r = F_{rrf} + F_{rsc} \quad (2)$$

The two criteria mentioned above can be mathematically expressed as follows:

$$[F_{rrf}]_{nonlinear\ part} = 0 \quad (3)$$

$$\frac{\partial}{\partial\phi_0}\int_0^{t_f} F_r dt = 0 \quad (4)$$

where t_f is the time when the particle exits the cavity of length L and ϕ_0 represents the phase of the RF when it leaves the cathode at $t = 0$. Which criterion to choose depends on which effect is dominant. In our case, because of relatively long bunches, we used the second criteria to design our cavities. We consider only the linear term in equation (2) which is dominant and regard the partial derivatives $\frac{\partial\beta_z}{\partial\phi_0}$, $\frac{\partial r}{\partial\phi_0}$ and $\frac{\partial t_f}{\partial\phi_0}$ as negligible. The following boundary conditions are assumed:

$$E_z(0,0) = E_0,\quad E_z(0,L) = 0,\quad \beta_0 \approx 0,\quad \omega t_f + \phi_0 = \pi \quad (5)$$

When trying to solve equation (4), it is natural to introduce some RF focusing near the cathode to help control the space charge effects. This can be expressed mathematically by writing:

$$\left.\frac{dE_z(0,z)}{dz}\right|_{z=0} = \frac{2m_0c^2k\cos\phi_0}{e^2rE_0\sin^3\phi_0}\int_1^{\gamma_f}\frac{F_{rsc}}{\beta_z}d\gamma \quad (6)$$

A sufficient condition to satisfy equation (4) is then:

$$\frac{d^2E_z(0,z)}{dz^2} = -k\cot(\omega t+\phi_0)\left(\frac{d\beta_z}{dz}E_z(0,z)+\beta_z\frac{dE_z(0,z)}{dz}\right) \quad (7)$$

where

$$\frac{d\beta_z}{dz} = \frac{(1-\beta_z^2)^{\frac{3}{2}}}{\beta_z}\frac{eE_z(0,z)}{m_0c^2}\sin(\omega t+\phi_0), \quad t = \frac{1}{c}\int_0^z \frac{dz}{\beta_z} \qquad (8)$$

Equation (7) together with conditions (5) and (6) can be solved numerically for given E_0, ϕ_0, current and cathode radius, provided that a simple linear expression is assumed for F_{rsc}. For the parameters of interest in our case, the resulting field distribution is shown in figure 1.

In the previous discussion, longitudinal emittance which is due to energy spread caused by time dependent RF forces was not minimized. By using a second cavity, it is possible to reduce energy spread while preserving emittance. For almost relativistic electrons, a cavity of length $L = \lambda/2$ having a field distribution $E_z(0,z) = E_1\sin(kz)$ satisfies both criteria [20]. It is then possible to almost cancel the energy spread by adjusting the maximum field E_1 and/or the phase shift between the two cavities ϕ_{12}. If $\phi_{12} = \pi - \Delta\phi/2$, then the field strength necessary to cancel the energy spread ΔW is:

$$E_1 = \frac{4k\Delta W}{e\pi\Delta\phi^2} \qquad (9)$$

If for other reasons, E_1 is set to a given value, then:

$$\phi_{12} = 2\pi - \phi_{1av} - \arcsin\left(\frac{2\Delta W}{E_1\lambda\sin(\frac{\Delta\phi}{2})}\right) \qquad (10)$$

where ϕ_{1av} is the average phase of the particles at the exit of the first cavity and λ is the RF wavelength.

Simulations

The two cavities shown on figure 2 were designed with SUPERFISH [21]. Being decoupled, each cell was calculated separately. The field profile as used for PARMELA simulations is shown on figure 1. After a slight modification of the PARMELA particle generation, it was shown that results obtained for 100 particles were reliable when compared to those corresponding to a much higher number. Therefore, all the simulations presented here were done with 100 particles. As the bunch is quite long and the current not too high, the mesh grid method is used for space charge calculations in order to save computer time. The effect of image charges in the cathode plane is not included in these simulations. A few parameters are not varied and their value are compiled in table 1. Electrons are assumed to leave the cathode with no energy and no emittance. The laser pulse is taken uniform in both transverse and longitudinal directions.

For given accelerating field and charge in the bunch the optimization procedure is as follows. The RF phase for laser pulse is varied to find the smallest emittance at the first cell exit. This phase is then frozen and the phase shift between the two cavities is varied to minimize the energy spread at the gun exit.

Figures 3 and 4 show the emittance at the exit of the first cavity, as a function of ϕ_0 for different field levels, with and without space charge forces respectively. ϕ_0 is the emitting RF phase of the "reference particle" which is taken at the center of the bunch. These pictures show that unlike for short bunches [22], the minimum of emittance is obtained for low ϕ_0 due to a strong bunching of the particles as shown on figure 5.

Figure 6 shows the dependence of emittance on peak accelerating gradient while figure 7 shows that the minimum emittance is quasi-linear with the bunch charge.

For a maximum electric field of 70 MV/m in both cavities, figure 8 shows the variation of both emittance and energy spread as a function of the phase shift between the two cavities.

A complete set of parameters for a typical run is given in table 2. Figure 1 shows the bunch evolution in this case as obtained from PRIAM. Both programs give consistent results.

In all these simulations, the emittance is taken as the normalized r.m.s. emittance defined as $\epsilon_N = 4[< x^2 >< (p_x/mc)^2 > - < x(p_x/mc) >^2]^{1/2}$ where x is the coordinate of a particle in the beam, p_x is the particle's momentum component in the x direction and $<\ >$ indicates averaging over the entire beam.

Project Status

Started in February 1990, the simulations with PARMELA and PRIAM will be continued. Different parameters will be scanned (shorter bunch length, magnetic field,...). Simulations in the case of a thermionic cathode are also in progress.

In order to check RF properties of the cavities and determine the two coupling holes, their influence on field symmetry and to check that cavities are effectively decoupled, a low-level model cavity was launched. Measurements will be done during the summer 1990.

Acknowledgement

We would like to thank Y. Thiery who performed all the simulation runs and B. Mouton who diligently modified PARMELA according to our wishes. Many thanks to Dr. J. Le Duff for his constant support.

References

[1] Version from K. Crandall and L. Young at LANL, with modifications from K.T. McDonald (BNL) and B. Mouton (LAL). User's manual from B. Mouton, LAL/SERA 89-356, 1989.
[2] G. Le Meur, these proceedings.
[3] J. Le Duff, in Proc. of the 1988 Linear Acc. Conf., Williamsburg, VA, October 3-7, 1988, pp. 285-287.
[4] G.A. Westenkow, J.M.J. Madey, Laser and Particle Beams (1984), Vol 2, Part 2, pp. 223-225.
[5] J. Gao, Beijing IHEP/FEL/89-04-(A,B,C,D),in chin., 1989.
[6] E. Tanabe et al., SLAC-PUB 5054, August 1989.
[7] R.L. Sheffield et al., Proc. of the 1988 Linear Acc. Conf., Williamsburg, VA, October 3-7, 1988, pp. 520-522.
[8] S. Joly, Proc. of the 1988 European Part. Acc. Conf., Rome, 1988.
[9] K.T. McDonald, DOE/ER/3072-43, Princeton University, 1988.
[10] M. Curtin et al., to be published in Proc. of the 1989 FEL Conf., 1989.
[11] S. Chattopadhyay et al., LBL-25699, ESG Note-55, 1988.
[12] Y. Baconnier et al., CLIC Note 65, 1988.
[13] W. Gai et al., Proc. of the 1989 Part. Acc. Conf., Chicago, 1989.
[14] H. Chaloupka et al., Nucl. Inst. and Methods in Phys. Res. A285 (1989), pp. 327-332.
[15] R. Bonifacio et al., Nucl. Inst. and Methods in Phys. Res. A289 (1990), pp. 1-13.
[16] G. Bienvenu, these proceedings.
[17] H. Bergeret, M. Boussonkaya, R. Chehab, B. Leblond, J. LeDuff, LAL/RT 90-04, 1990.
[18] B.E. Carlsten, R.L. Sheffield, Proc. of the 1988 Linear Acc. Conf., Williamsburg VA, October 3-7, 1988, pp. 365-369.
[19] M.E. Jones, W.K. Peter, IEEE Trans. on Nucl. Sci., Vol NS-32, No 5, p. 1794, 1985.

[20] J. Gao, LAL/SERA 89-291, Orsay, August 1989.
[21] K. Halbach, R.F. Holsinger, Proc. of the 1976 Part. Acc. Conf., pp. 213-222
[22] K.J. Kim, Y.J. Chen, Proc. of the 1988 European Part. Acc. Conf., Rome, 1988.

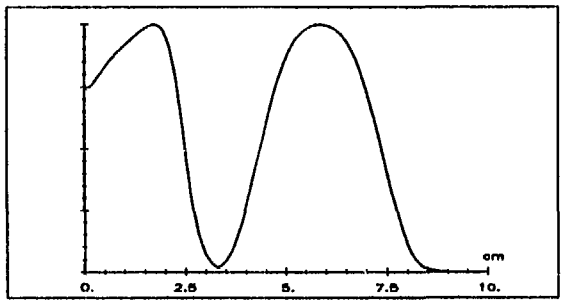

Fig. 1: Longitudinal on-axis electric field

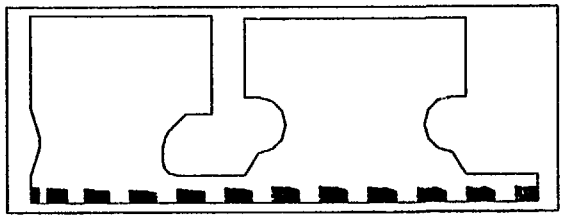

Fig. 2: Cavity contour

Table 1
Fixed parameters during simulations

Laser pulse length (ps)	30.
Laser spot radius (mm)	3.
RF Frequency (GHz)	3.
First cell length (cm)	3.325
Second cell length (cm)	5.835
Cell aperture radius (mm)	5.
Emittance at cathode (mm.mrd)	0.
Magnetic field (T)	0.

Table 2
Parameters for a typical run

Number of particles	100	
Charge in a bunch (nC)	2.	
RF phase for laser pulse (deg.)	22.	
Phase shift between cavities (deg.)	150.	
	1^{st} cell	2^{nd} cell
Max. electric field (MV/m)	70.	70.
Kinetic energy (MeV)	1.326	2.867
Bunch length (ps)	17.	17.
Peak current (A)	118.	118.
Bunch radius (r_{max}) (mm)	3.1	3.9
Energy spread (KeV)	186.	33.
Energy spread (%)	14	1.1
Emittance (mm.mrd)	27.3	34.2
Emittance (RF) (mm.mrd)	18.7	15.5
Angular divergence (mrd)	44.7	24.2

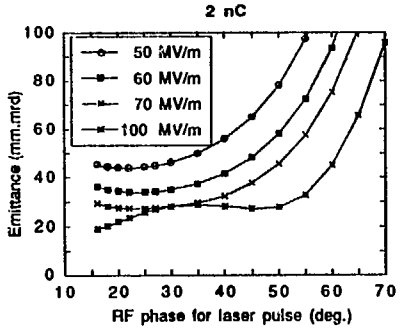

Fig. 3: Emittance after the first cell vs. ϕ_0 for a 2 nC bunch

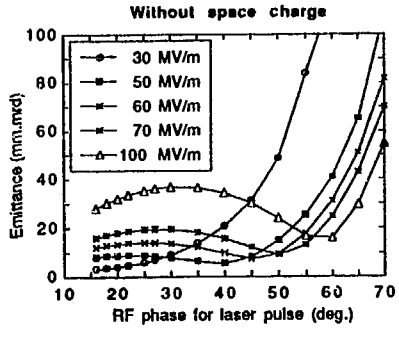

Fig. 4: Emittance after the first cell vs. ϕ_0 when space charge effect is not included

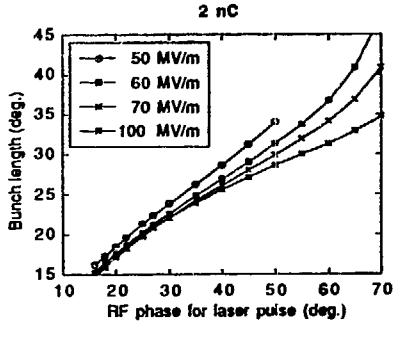

Fig. 5: Bunch length after the first cell vs. ϕ_0

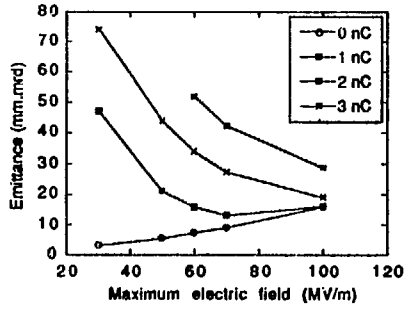

Fig. 6: Emittance after the first cell vs. the maximum electric field

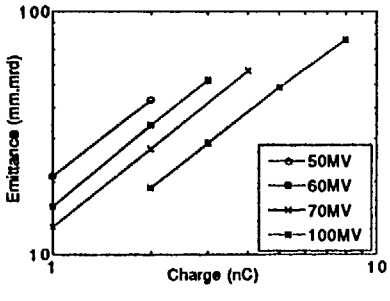

Fig. 7: Emittance after the first cell vs. bunch charge

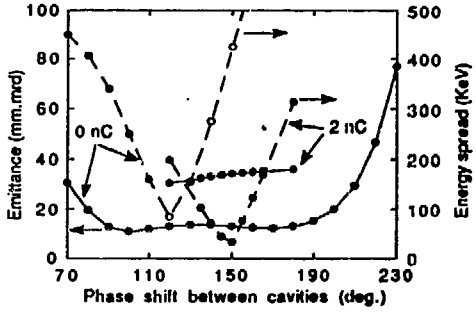

Fig. 8: Emittance and energy spread after the second cell vs. the phase shift between the two cavities